



HAL
open science

Evolution of superflares of H₂O maser emission in IRAS 16293-2422

Pierre Colom, N. T. Ashimbaeva, E. E. Lekht, M. I. Pashchenko, G. M.
Rudnitskij, V. V. Krasnov, A. M. Tolmachev

► **To cite this version:**

Pierre Colom, N. T. Ashimbaeva, E. E. Lekht, M. I. Pashchenko, G. M. Rudnitskij, et al.. Evolution of superflares of H₂O maser emission in IRAS 16293-2422. Monthly Notices of the Royal Astronomical Society, 2021, 507, pp.3285-3291. 10.1093/mnras/stab2287 . insu-03713746

HAL Id: insu-03713746

<https://insu.hal.science/insu-03713746>

Submitted on 14 Apr 2023

HAL is a multi-disciplinary open access archive for the deposit and dissemination of scientific research documents, whether they are published or not. The documents may come from teaching and research institutions in France or abroad, or from public or private research centers.

L'archive ouverte pluridisciplinaire **HAL**, est destinée au dépôt et à la diffusion de documents scientifiques de niveau recherche, publiés ou non, émanant des établissements d'enseignement et de recherche français ou étrangers, des laboratoires publics ou privés.

Evolution of superflares of H₂O maser emission in IRAS 16293–2422

Pierre Colom,¹ N. T. Ashimbaeva,² E. E. Lekht,^{2*} M. I. Pashchenko,² G. M. Rudnitskij,² V. V. Krasnov³ and A. M. Tolmachev⁴

¹LESIA, Observatoire de Paris, Section de Meudon, CNRS, UPMC, Université Paris–Diderot, 5 place Jules Janssen, 92195 Meudon Cedex, France

²Lomonosov Moscow State University, Sternberg Astronomical Institute, 13 Universitetskij prospekt, Moscow 119234, Russia

³Astro Space Center, Lebedev Physical Institute, Russian Academy of Sciences, 53 Leninskij prospekt, Moscow 119991, Russia

⁴Pushchino Radio Astronomy Observatory (PRAO), Astro Space Center, Lebedev Physical Institute, Russian Academy of Sciences, Pushchino, Moscow region 142290, Russia

Accepted 2021 August 3. Received 2021 August 2; in original form 2021 March 10

ABSTRACT

The aim of this work was to continue the monitoring of the H₂O maser emission in IRAS 16293–2422 to detect superflares. We have been observing H₂O maser emission at a wavelength of 1.35 cm towards the source IRAS 16293–2422 since 1999. The observations have been carried out with the 22-m radio telescope of the Pushchino Radio Astronomy Observatory (Russia). In 2007–2018, we also conducted several sessions of observations in OH lines at a wavelength of 18 cm in both circular polarizations with the Nançay Radio Telescope (France). Between 1997 and 2021, we observed three cycles of high activity of the H₂O maser with a period of 8 yr. This variability could be related to the changing activity of the protostar in the tight binary system of IRAS 16293–2422 in the process of its formation. This variability could be related to an increase in the activity of the tight binary protostar IRAS 16293–2422 A, first seen in 2002. The H₂O maser variation in flux density and radial velocity suggests that disturbances are propagating through organized structures in the form of chains ~ 3.5 au long, with monotonic velocity gradients in the direction of propagation. The 18-cm OH emission in the main and satellite lines is thermal.

Key words: masers – star: activity – stars: formation – ISM: jets and outflows.

1 INTRODUCTION

The source IRAS 16293–2422, which has a complex structure, is located in the ρ Oph dark cloud. This is a typical old infrared source. It presents very rich spectra with numerous complex molecules, indicating a particularly active chemistry. IRAS 16293–2422 happens to be one of the first very young multiple stellar systems ever identified.

The system is at a distance of 120 pc from the Earth (Knude & Hog 1998). The distance estimated from its annual parallax is 180 pc (Imai et al. 2007) or 140 pc (Dzib et al. 2018). The estimated bolometric luminosity of IRAS 16293–2422 is $\approx 21 L_{\odot}$ (Jacobsen et al. 2018). Observations of Wilking & Lada (1983) in the C¹⁸O line showed that the central part of the cloud (core) has a size of 2 pc. The dynamical mass of the molecular core is about $2.3 M_{\odot}$, and the core density exceeds 10^8 cm^{-3} . Interferometric observations of the infrared source at a wavelength of 2.7 mm revealed a disc structure with a size of $1800 \text{ au} \times 800 \text{ au}$ (Mundy et al. 1992).

IRAS 16293–2422 is a binary system with components A and B separated by 5 arcsec (700 au) and is embedded in the dense molecular core (see e.g. Looney, Mundy & Welch 2000; Chandler, Brogan & Loinard 2005). Source A represents at least two major outflows: an east–west bipolar CO molecular outflow at a radial velocity of 4 km s^{-1} (Yeh et al. 2008); and a compact SiO outflow (Rao et al. 2009).

Mundy et al. (1992) confirmed the protostellar nature of A and B by detecting compact thermal 3-mm emission coinciding with the position of the cm sources. Source B has a simple structure from cm to submm waves; it is believed that it may be at a very early stage of evolution and may not even have begun a phase of significant mass loss. Source A is double and consists of components A1 and A2, which are separated from each other by 0.34 arcsec. The emission from A2 is resolved and traces a dusty circumstellar disc with a full width at half-maximum (FWHM) size of 12 au (Maureira et al. 2020). Component A1 is not resolved, and the limiting size of the dust circumstellar disc is 3.6 au.

Chandler et al. (2005) found that at the position of component A there are in fact two submm sources, Aa and Ab. The peak of the emission of the strongest of them, denoted as Aa, is located between the cm radio sources A1 and A2. Relative movement between them has been detected. Most likely, two protostellar objects are moving in a Kepler orbit. Thus the A1/A2 pair is a tight binary system. Subsequent VLA (Very Large Array of the National Radio Astronomy Observatory) and ALMA (Atacama Large Millimeter/Submillimeter Baseline Array) observations confirmed both absolute and relative movements of sources A1 and A2 (Hernández-Gómez et al. 2019; Maureira et al. 2020). In this case, the individual masses of protostars are estimated as $\sim 0.8 M_{\odot}$ and $\sim 1.4 M_{\odot}$ for A1 and A2, respectively (Maureira et al. 2020).

According to Pech et al. (2010), 2005 was the beginning of the bipolar ejection of components A2 α and A2 β from the protostar A2, and these components began to disperse symmetrically relative to A2. The expansion velocity of the components was $30\text{--}80 \text{ km s}^{-1}$.

* E-mail: eelekht@mail.ru

With sufficient separation of components A2 α and A2 β , the source A2 became visible again.

H₂O maser emission was detected by Wilking & Claussen (1987). Then, according to observations in 1987, Terebey et al. (1992) showed that H₂O maser emission comes from a 0.6-arcsec region (96 au) and that it is associated solely with source A. According to Alves et al. (2012), H₂O maser emission is localized near source Aa. None of the multiple molecular outflows, nor the H₂O maser emission, is associated with source B. Monitoring carried out by Furuya et al. (2003) from late 1997 up to mid-1998 demonstrated the rapid variability of H₂O maser emission with a time-scale of a few days. Imai, Iwata & Miyoshi (1999) mapped H₂O maser spots for three epochs in 1991 and 1994. They also detected the proper motions of 10 maser spots within a time interval from the end of 2003 up to the end of 2004 (Imai et al. 2007). Three of them are discussed in detail. Later, from 2005 August to 2006 April, Dzib et al. (2018) performed similar parallax observations for three maser spots with Very Long Baseline Array (VLBA) for 13 epochs. Using the VLA (NRAO), Alves et al. (2012) measured the linear polarization of the H₂O maser at $\lambda=1.35$ cm and Zeeman splitting that correspond to a strong magnetic field (113 mG). They suggested that the magnetic field is energetically important in the dynamical evolution of IRAS 16293–2422.

Very strong, short-lived features appeared at blue- and redshifted velocities with respect to that of the CO molecular cloud (4 km s⁻¹). According to Colom et al. (2016), H₂O maser variations demonstrate a sequence of powerful flares, occasionally reaching tens of kilojanskys.

Towards IRAS 16293–2422, unpolarized emission in the main OH lines of 1665 and 1667 MHz was observed (Pöppel & Scalise 1989; Colom et al. 2016). Methanol maser emission was not detected (Slysh et al. 1999). The absence of hydroxyl and methanol maser emission as well as of a radio continuum are typical for very young objects. And since there is no maser emission of methanol at a frequency of 6.7 GHz, this supports the assumption that the protostars in IRAS 16293–2422 are low-mass.

Finally, we note that according to van der Wiel et al. (2019), IRAS 16293–2422 represents a special stage in the evolution of binary star systems. Many other protostars may pass through this phase at some stage of their evolution. The tight binary A1/A2 pair and component B in IRAS 16293–2422 represent a very young hierarchical multiple system (Pech et al. 2010).

2 OBSERVATIONS

We have been observing H₂O maser emission at a wavelength of 1.35 cm towards the source IRAS 16293–2422 since 1999. The observations have been carried out with the 22-m radio telescope of the Pushchino Radio Astronomy Observatory, Lebedev Institute of Physics, Russian Academy of Sciences. The telescope sensitivity for a point-like unpolarized source is 25 Jy K⁻¹. The system noise temperature is from 130 to 250 K, depending on the observing conditions. The aerial half-power beamwidth (HPBW) is 2.6 arcmin. The signal was recorded by a 2048-channel autocorrelation spectrum analyser with a velocity resolution of 0.0822 km s⁻¹. All the spectra have been corrected for absorption in the Earth’s atmosphere. Until 2018 March, we took the velocity of the Sun’s motion to be 19.5 km s⁻¹. After 2018 March took it to be 20 km s⁻¹. Therefore, we have corrected the radial velocity scale of all spectra as well as of those previously observed and used in this work.

In this paper, we use previously published observational data (Colom et al. 2016) and new observations made in 2015–2021.

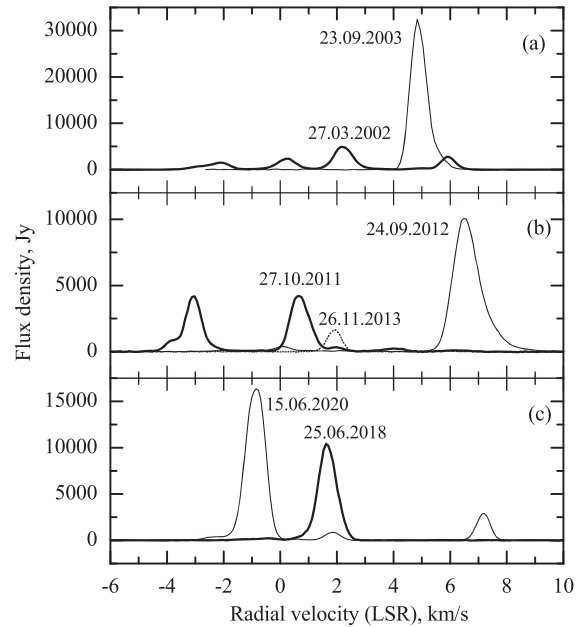


Figure 1. Selected H₂O spectra in different epochs of observations. In all the figures and in the text, the values of the radial velocity are given relative to the local standard of rest.

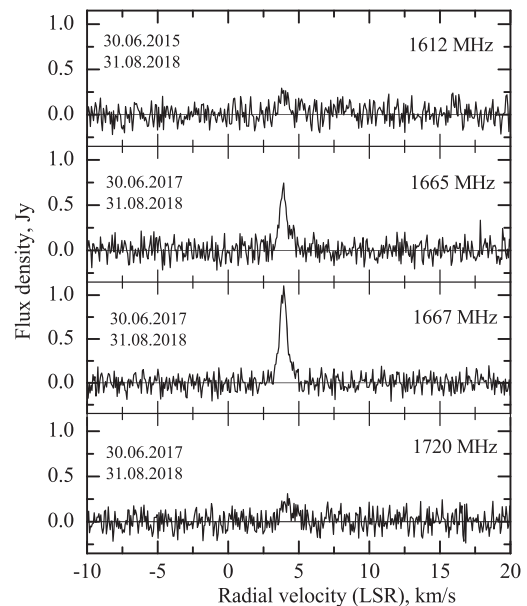


Figure 2. OH line spectra averaged over two epochs (2017 June 30 and 2018 August 31) measured at the Nançay Radio Telescope.

Sample H₂O spectra for various epochs of observations are shown in Fig. 1. For each activity cycle (see Fig. 3), two or three spectra with different emission levels were selected.

In 2007–2018, we also conducted several sessions of observations in OH lines at a wavelength of 18 cm in both circular polarizations at the Nançay Radio Telescope (France). The system noise temperature was 35–60 K, depending on the observing conditions. The spectral resolution was 0.0682 km s⁻¹. OH line spectra averaged over two epochs (2017 June 30 and 2018 August 31) are given in Fig. 2. The total integration time was 70 min, giving a noise level in a single polarization of about 100 mJy.

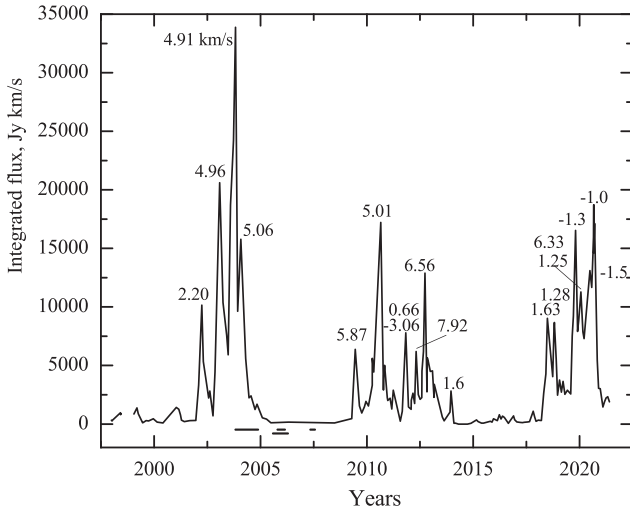


Figure 3. Integrated flux variations of H₂O maser emission in IRAS 16293–2422. Radial velocities of the main flare features are indicated above each peak. At the bottom, the segments of horizontal lines mark the time intervals of VLA (Imai et al. 2007), VLBI Exploration of Radio Astrometry (VERA) (Alves et al. 2012), and VLBA (Dzib et al. 2018) observations.

3 DISCUSSION

The results of our previous observations of 1999–2015 showed that the H₂O maser emission in IRAS 16293–2422 demonstrates a sequence of powerful flares, with the flux density occasionally reaching tens of kilojanskys. In 2019 and 2020, even stronger flares were detected.

We compare the results of the evolution of these flares with the proper movements of individual maser spots measured by Imai et al. (2007) and Dzib et al. (2018). We discuss the observed radial velocity drifts of such spots, which are not necessarily due more to the acceleration or deceleration of the massive gas. This may also be due to the passage of the shock wave through a chain of successive gas clumps with different radial velocities.

3.1 Integrated flux

The H₂O maser source IRAS 16293–2422 is characterized by strong flares. It is of interest to associate this property with the overall activity of the source. Integrated flux is an important parameter maser emission. Fig. 3 shows variations of this parameter for 1997–2021. We have also included the data of Furuya et al. (2003) obtained at the Nobeyama 45-m telescope from 1997 December to 1998 June. Earlier observations obtained by Wilking & Claussen (1987) in 1986–1987 and by Terebeyet al. (1992) of the integrated flux did not exceed ~ 700 Jy km s⁻¹.

There have been three cycles of very high activity of the H₂O maser, separated by long intervals of considerably lower activity. In each activity cycle, strong flares with one or several emission features were observed. In Fig. 3, each flux peak is labelled with the radial velocities of the main flaring features. In the third cycle, in addition to the superflare, there were flares of H₂O emission at several radial velocities (see Fig. 3). This implies an increase in the activity of the entire H₂O maser, not of an individual maser spot. The period of activity was 8 yr.

Fig. 4 shows the radial velocity of the main features in the epochs of their emission maxima. Let us call these the peak velocities. As a rule, they coincide with the maxima of the integrated flux. It can

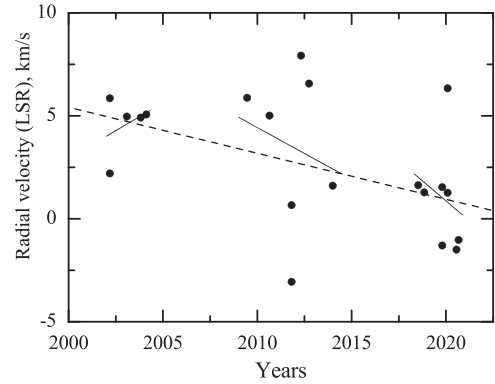


Figure 4. Radial velocity of the main features in the epochs of their emission maxima. The segments of the solid lines and the dashed line show the trend of displacement of the V_{LSR} emission maxima for each activity cycle and the entire observation period (2000–2021), respectively.

be seen that there is a tendency for the radial velocity of the most intense emission to decrease over time, which is approximated by a straight line.

At the beginning of the first cycle of activity in 2002, a strong flare occurred at 2.2 km s⁻¹ (with a flux of about 5000 Jy), and at the same time strong emission was observed at velocities of -2.04 and 0.26 km s⁻¹ (see Fig. 1, spectrum of 27.03.2002). The emission was relatively short-lived. According to Imai et al. (2007) and Dzib et al. (2018), a maser spot at a velocity of 2.1 km s⁻¹ is located ~ 0.2 arcsec south-east from the continuum source A2, roughly in the middle of A1 and A2. There is also an outflow from the protostar. We can assume that the flare we are observing is related to this maser spot and is associated with shocks in the outflow.

VLBI Expolaration of Radio Astrometry (VERA) observations in 2003 October almost coincided with the maximum of the strong flare, when the flux density reached almost 50 000 Jy. In this epoch, the maser spot had a radial velocity of 4.3 km s⁻¹. The type of variability of this emission obtained in our monitoring is similar to that in Imai et al. (2007) (feature *a*): a split into two components, an increase in the radial velocity, and large fluxes. So it is the same feature. According to Imai et al. (2007), this maser feature is probably associated with the outflow.

Finally, when the flash ended, the maximum emission velocity in 2005–2006 was 6.1 km s⁻¹ (Dzib et al. 2018), and in mid-2007 it reached 7.4 km s⁻¹ (Imai et al. 2007). Thus, there was a regular increase in the radial velocity of the strongest emission. From monitoring by Colom et al. (2016) and observations by Imai et al. (2007) for 13 epochs, it is obvious that we are dealing with the same maser spot or cluster of spots (e.g. a chain with a radial velocity gradient along it). We analysed the first observations of the H₂O maser in IRAS 16293–2422 (1987–1994) and obtained a similar result. The identical nature of the variability of this maser emission in different epochs can be in the case when it is associated with the same cluster of maser spots.

The second cycle of activity differs greatly from the first, primarily in the width of the emission spectrum (from -5 to $+10$ km s⁻¹). A more significant difference is that strong maser emission was consistently observed in different parts of the spectrum. This is apparent in the inset in Fig. 3. It is likely that this emission is associated with different clusters of maser spots under non-stationary (quasi-periodic) and non-isotropic action, for example of a shock wave from a protostar.

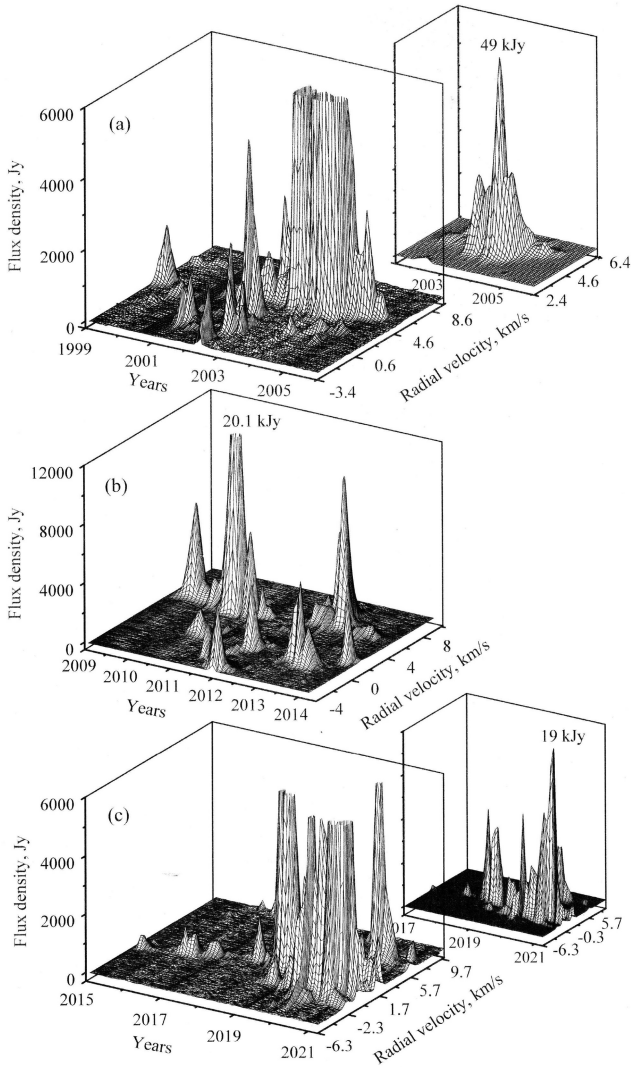


Figure 5. 3D representation of the H₂O maser emission spectra of IRAS 16293–2422 for three activity cycles.

In the third cycle of activity, the observed spectrum covers the full range of velocities at which flares have been detected, from -6 to 15 km s⁻¹, but since 2015 superflares mostly occurred in the range of radial velocities from -4 to 3 km s⁻¹, and only for a little more than half a year (2019 August–2020 March), in the velocity range 6 – 9 km s⁻¹ (see Fig. 3).

Analysis of maser emission at $V < 0$ km s⁻¹ from 1991 to 2021 shows that there is also a cyclic nature of the variability of this emission, with a period close to 8 yr. According to Imai et al. (1999), maser spots with a blue velocity shift are associated with the region of interaction of a bipolar flow with a rotating gas–dust disc.

The periodic variability of H₂O maser emission with a time-scale of 8 yr may be related to the activity of the protostar in the binary system A1–A2 of IRAS 16293–2422 in the process of its formation.

Fig. 5 provides a 3D representation of the H₂O maser emission spectra of IRAS 16293–2422 for three activity cycles. For the first and third activity cycles, the 3D image is shown at two different scales. This figure illustrates well the flare character of the H₂O maser emission during the entire observation period of IRAS 16293–2422.

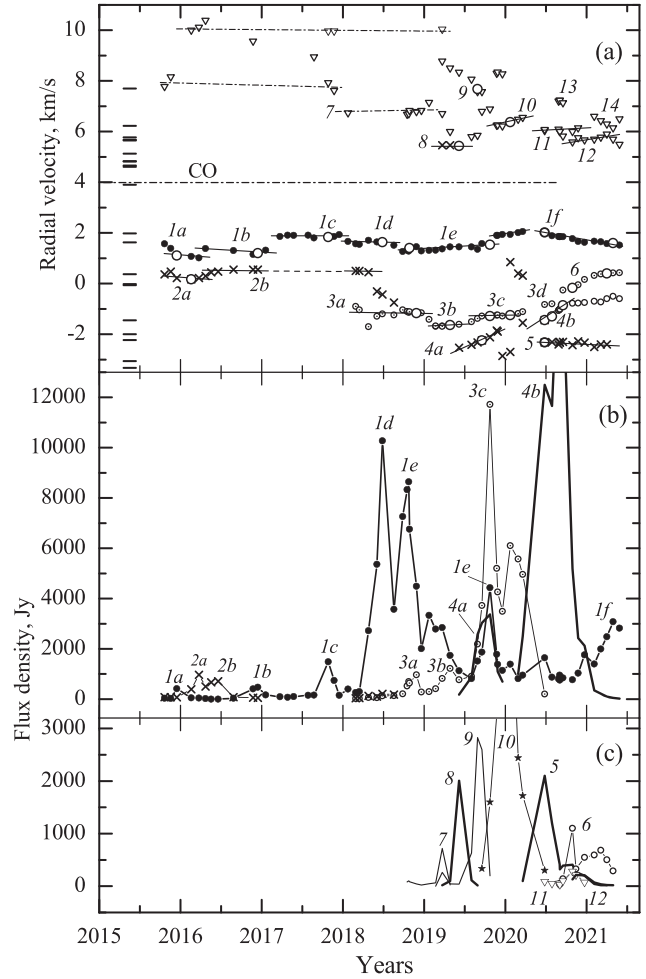


Figure 6. (a) Radial velocity and (b) flux density variations of H₂O emission features for cycle 3; (c) shows weaker flares in the same period as (b). The results of a similar analysis up until 2015 were published by Colom et al. (2016). Segments of straight lines connect points with similar radial velocities. The emission features with flux densities above 1500 Jy observed by us in 1999–2015 are given on the left (a). The dash–dotted line shows the velocity of the CO molecular cloud, 4 km s⁻¹.

3.2 Individual emission features

Fig. 6 shows variations of the radial velocity (a) and flux density (b) of the main spectral features. Segments of straight lines connect points with similar radial velocities. The positions of emission features with flux densities that exceeded 1500 Jy in the interval of our observations 1999–2015 are given on the left. The dot–dashed line shows the velocity of the CO molecular cloud, 4 km s⁻¹.

During one year (end of 2003–end of 2004), Imai et al. (2007) carried out multi-epoch very long baseline interferometry (VLBI) observations. They detected the proper motions of 10 maser spots. Much attention was paid to the study of the maser spots at 4.43, 2.79, and 2.02 km s⁻¹. The reference feature a, at 4.43 km s⁻¹, has a proper motion of -13.1 , -16.3 mas in R.A. and Dec. with respect to IRAS 16293–2422 A2 (Hernández-Gómez et al. 2019). Within our monitoring program, we observed IRAS 16293–2422 at the same epochs, and also observed these emission features (Colom et al. 2016). The emission of the maser spot at 4.43 km s⁻¹ was the strongest. Its flux density was as high as 45 000 Jy. By the end of 2004, its radial velocity had increased to 5.2 km s⁻¹.

In the next activity cycle, the emission near 5.2 km s⁻¹ was observed only up to 2013. The most powerful emission in the form of the consecutive flares of four individual features took place in 2009–2010. Thus it was the maser spot whose drift in 2003–2004. One of the causes may be the decay of the spot into several components. Another reason may be the non-isotropic and variable outflow of material from the protostar.

As noted above, since 2016 in the radial-velocity interval 2.3–6 km s⁻¹ we have not observed emission with a flux density above 5 Jy. The highest activity of the water vapour maser moved in velocity from 5.2 to ~1.5 km s⁻¹. The emission near 2 km s⁻¹ had been observed since the detection of the H₂O maser in IRAS 16293–2422. According to Imai et al. (1999), the maser spots in the radial-velocity intervals 1–4 and 4–7 km s⁻¹ were localized in different parts of the source, and this type of variability could be associated with an inhomogeneous and irregular outflow of matter from the protostar. The intensity of the redshifted outflow hosting maser spots with velocities 4–6 km s⁻¹ could decrease (see e.g. Dzib et al. 2018).

The third activity cycle can be divided into two stages: pre-superflare and the superflare itself. In the first stage, we observed emission in the velocity range from -0.6 to 2.3 km s⁻¹. Then, with a time delay, two consecutive flares occurred at 0.4 and 1.2 km s⁻¹ with flows of 900 and 400 Jy, respectively (see Fig. 6, features 2a and 1a). There was a slight speed drift. For feature 2a, the drift was +0.3, and for feature 1a, it was -0.3 km s⁻¹.

Subsequently, we observed that feature 1 was persistent, with numerous small jumps in the radial velocity. Feature 2 was detected only up to the end of 2016 and for a short time in early 2018.

The superflare was preceded by a flare at a velocity of 1.89 km s⁻¹ with a peak flux density of 1490 Jy (see Fig. 6, feature 1c). Then the velocity jumped to 1.63 km s⁻¹. At precisely this velocity we observed powerful emission with a peak flux density of 10 200 Jy (feature 1d). At the time of a sharp decrease in the flux density, the velocity jumped again from 1.63 to 1.34 km s⁻¹, and a new flare occurred (feature e). Thus, the velocity jumps were -0.26 and -0.30 km s⁻¹, respectively. The time intervals during which the velocity jumps occurred can be estimated as ~0.15 yr. Probably, three maser spots having close radial velocities were consecutively excited by a shock wave.

The delays between the flux density maxima of these features were 0.67 and 0.31 yr. The maser could be pumped by a shock wave. For instance, Ristorcelli et al. (2005) found evidence for a shock in IRAS 20126+4104 in the data on submm emission in water vapour lines.

Kaufman & Neufeld (1996) modelled these data and showed that in the vicinity of the source IRAS 20126+4104 there may exist a C-type (continuous) shock with a velocity of 12–15 km s⁻¹. We adopt a velocity of 15 km s⁻¹. Then the delays of 0.67 and 0.31 yr found in our observations of IRAS 16293–2422 correspond to a spatial separation between the features (perpendicular to the shock front) of 2.1 and 1 au and to a total chain length of ~3–3.5 au. This is consistent with the results obtained for the superflares of the second activity cycle in 2009–2014, as well as for other sources, for example W75N (Lekht et al. 2007; Torrelles et al. 1997).

At the end of 2019, a second superflare occurred at a radial velocity of -1.3 km s⁻¹. It was more powerful, with a maximum flux density of 11 700 Jy, but more short-lived, and it was associated with chain feature 3. In 2020 June, we registered a new superflare with a flux density of 12 500 Jy (feature 4b). The evolution of this flare and of the spectrum structure are complex (see Fig. 7). There is a significant

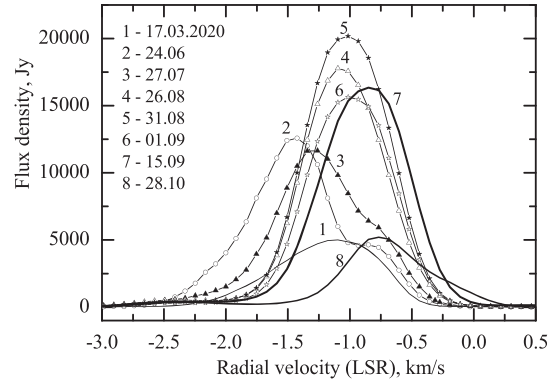


Figure 7. Superposition of spectra of the superflare for various epochs of observations (feature 4b). They are numbered in chronological order (top left).

drift of the maximum emission along the radial velocity. The drift rate was 0.22 km s⁻¹ mon⁻¹.

Throughout our monitoring of IRAS 16293–2422 we also observed features that were active for a short time, 1–3 months. These are often called short-lived features. They were most numerous in the velocity interval between -3.5 and 1.6 km s⁻¹, and had flux densities up to 4200 Jy. A lower number of such features appeared in the velocity interval 7.2–9.5 km s⁻¹. Their flux densities were lower and did not exceed 700 Jy. Such flares can occur in the presence of small-scale turbulent movements in the medium.

A very short flare occurred in 2019 June at 5.4 km s⁻¹, with a flux density of more than 2000 Jy (Fig. 6, feature 8). In 2019 December–2020 March at an average velocity of 6.3 km s⁻¹, a longer strong emission was observed, with a flux density with a maximum of 6250 Jy (feature 10). There was a radial velocity drift. The line was symmetrical, and its width was about 0.6 km s⁻¹ and changed very slightly during the total drift. All this shows that the flare feature was single. Most likely, the maser spot responsible for this emission is a filament along which the radial velocity changes monotonically.

3.3 Hydroxyl emission

The high sensitivity of our observations of hydroxyl lines allowed us to detect two components in the spectra of all four OH lines (see Fig. 2). We fitted two spectral Gaussians to separate the components.

The radial velocity of the main component is almost the same for all four lines, both main and satellite lines, and is equal to 3.9 ± 0.05 km s⁻¹. The flux densities are 0.24, 0.65, 1.04, and 0.19 Jy for the lines at 1612, 1665, 1667, and 1720 MHz, respectively. The ratio of fluxes is equal to 1.3 : 3.4 : 5.5 : 1. This is slightly different from the classical ratio for thermal emission. The width line emission of the component is in all cases about 0.65 km s⁻¹. In this case, the temperature for the region of hydroxyl emission is ~30 K.

The second, weaker component was also observed in all four OH lines. The spread of fluxes was less than that of the main component, only 1.5 times. However, there was a large difference in the radial velocity value, from 4.6 to 5.1 km s⁻¹. In principle, this may to some extent be the result of an error in measuring the speed of a weak signal. We estimate the line width of this component as 0.5 km s⁻¹.

The measured parameters of OH emission indicate that this emission is thermal and that the medium where this emission occurs is inhomogeneous. It would be of interest to conduct observations in satellite lines with higher sensitivity to confirm the difference in

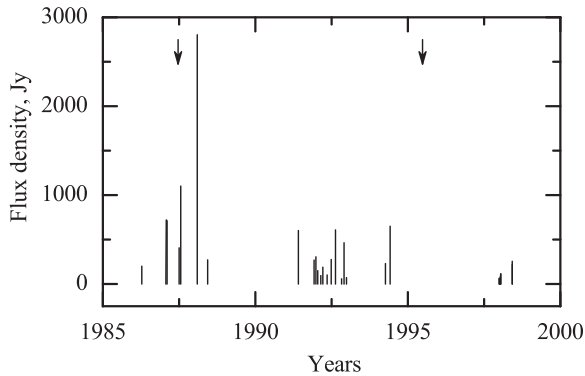


Figure 8. The main features of the spectra of H₂O for IRAS 16293–2422 for various epochs of observations in 1986–1998 (see text). The vertical arrows show the midpoints of the expected maser activity cycles.

the radial velocities in the main and satellite lines of the second component and to identify the nature of this phenomenon.

3.4 About the H₂O maser model

Recall that A1 is a protostar, not a shock function, and the A1/A2 pair is a bound binary system. Source IRAS 16293–2422, including B, therefore appears to be a very young hierarchical multiple structure (Pech et al. 2010). The 3-mm ALMA continuum observations toward IRAS 16293–2422 A showed that the emission A2 is resolved and traces a dust disc with a FWHM size of ~ 12 au and protostar mass of $\sim 1.4 M_{\odot}$ (Maureira et al. 2020). Specifically, the water vapour maser (maser spot) with $V_{\text{LSR}} = 6.1 \text{ km s}^{-1}$ is associated with the redshifted lobe of the outflow with positional angle (PA) = 110° (Dzib et al. 2018).

According to Pech et al. (2010), 2005 was the beginning of the bipolar ejection of components A2 α and A2 β from A2, which begin to disperse symmetrically relative to A2. The expansion velocity of the components was 30–80 km s^{-1} . With sufficient separation of components A2 α and A2 β , the source A2 became visible again. Shortly before this event, since 2002, there was a significant increase in the activity of the water vapour maser, and a series of superflares occurred (Colom et al. 2016).

There were three such series of superflares with a period of 8 yr. The question arises, what happened before 2002? To address this question, in Fig. 8 we plot the main features of each spectrum obtained before our monitoring, from 1986 to 1998 (Wilking & Claussen 1987; Wootten 1989; Terebey et al. 1992; Pöppel & Scalise 1989; Imai et al. 1999; Furuya et al. 2003).

It is possible to extrapolate back in time the positions of the maser activity cycles with a period of 8 yr, which are obtained in this work. The midpoints of the epochs of the assumed activity cycles are marked with vertical arrows.

In 1986–1988, the main emission in the spectrum occurred at radial velocities in the range of 6.2–7.0 km s^{-1} with a flux density from 700 to 2800 Jy. This is quite strong emission, but more than 20 times weaker than during superflares. In 1994–1996, there were only two observations, by Imai et al. (1999). In 1994, they observed strong emission at a velocity of 1.9 km s^{-1} with a flux density of 230 Jy (April 5) and 650 Jy (June 1). Between the activity cycles (1992 and 1998), the emission was weaker (see Fig. 8). Comparing all the results of H₂O observations in IRAS 16293–2422 before 2002 and after, we can say that super-powerful emission (superflares) began to occur only after 2002.

A significant increase in the activity of the water vapour maser and a series of superflares precede the bipolar outflow of components A2 α and A2 β from the A2 source. It can be assumed that all this is due to an increase in the activity of the protostar since 2002.

We pay attention to two important factors. During the evolution of the main maser feature at $\sim 5 \text{ km s}^{-1}$ in 2003–2004, not only its proper motion was observed, but also its bifurcation and change in radial velocity (see Imai et al. 2007, fig. 2). According to monitoring data, Colom et al. (2016) showed that in 2003–2004 there was a drift of H₂O velocity emission from 4.3 to 5.3 km s^{-1} . It was associated with the flares. In this case, there was a successive excitation by a shock wave spatially exploded features in a structure, for example in the form of a chain. In this case, the shock wave successively excited spatially distinct features such as in a chain. Thus, different features of the chain are observed one after another at different epochs.

These two observed phenomena show the existence of a mechanism for the shock excitation of maser emission and the presence of a complex structure in maser spots. As shown by Imai et al. (2007) and Colom et al. (2016), these factors can affect the results of measurements of the proper motions of maser spots and the magnitude of the trigonometric parallax.

4 CONCLUSIONS

The main results obtained from our monitoring of the source IRAS 16293–2422 in the H₂O line at a wavelength of 1.35 cm are as follows.

(i) Between 1997 and 2021 we observed three cycles of high activity of the H₂O maser with a period of 8 yr. We related this variability to the changing activity of the protostar in a tight binary system of IRAS 16293–2422 A in the process of its formation. There is a tendency to shift the maser activity towards lower radial velocities.

(ii) The maser emission of water vapour is a superposition of strong flares of mostly single features (often short-term) with flux densities above 10 000 Jy. The line profiles are usually asymmetrical, and the line wings are sometimes blended emission from weaker features.

(iii) The character of the variability of the flux density and radial velocity suggests that individual H₂O maser features can form organized structures in the form of chains ~ 3.5 au long, with a monotonic variation of radial velocity along them.

(iv) In the main (1665- and 1667-MHz) and satellite (1612- and 1720-MHz) lines of OH molecules, the radio emission is unpolarized and thermal. The presence of the second component in the OH spectra shows that the medium for generating this emission is inhomogeneous. The line width of the main component is 0.65 km s^{-1} , which is possible at a medium temperature of about 30 K.

(v) A significant increase in the activity of the water vapour maser and a series of superflares precede the bipolar ejection of components A2 α and A2 β from the A2 source. It can be assumed that all this is due to an increase in the activity of the protostar since 2002.

ACKNOWLEDGEMENTS

The authors are grateful to the staff of the Pushchino and Nançay radio observatories for their help with the observations.

DATA AVAILABILITY

The data underlying this article are available in the article.

REFERENCES

- Alves F. O., Vlemmings W. H. T., Girart J. M., Torrelles J. M., 2012, *A&A*, 542, A14
- Chandler C. J., Brogan C. L., Shirley Y. L., Loinard L., 2005, *ApJ*, 632, 371
- Colom P., Lekht E. E., Pashchenko M. I., Rudnitskii G. M., Tolmachev A. M., 2016, *Astron. Rep.*, 60, 730
- Dzib S. A. et al., 2018, *A&A*, 614, A20
- Furuya R. S., Kitamura Y., Wootten A. Claussen M. J., Ryohei R., 2003, *ApJS*, 144, 71
- Hernández-Gómez A. et al., 2019, *ApJ*, 875, 94
- Imai H., Iwata T., Miyoshi M., 1999, *Publ. Astron. Soc. Japan*, 51, 473
- Imai H. et al., 2007, *Publ. Astron. Soc. Japan*, 59, 1107
- Jacobsen S. K. et al., 2018, *A&A*, 612, A72
- Kaufman M. J., Neufeld D. A., 1996, *ApJ*, 456, 250
- Knude J., Hog E., 1998, *A&A*, 338, 897
- Lekht E. E., Slysh V. I., Krasnov V. V., 2007, *Astron. Rep.*, 51, 967
- Looney L. W., Mundy L. G., Welch W. J., 2000, *ApJ*, 529, 477
- Maureira M. J., Pineda J. E., Segura-Cox D. M. Caselli P., Testi L., Lodato G., Loinard L., Hernández-Gómez A., 2020, *ApJ*, 897, 59
- Mundy L. G., Wootten A., Wilking B. A. Blake G. A., Sargent A. I., 1992, *ApJ*, 385, 306
- Pech G., Loinard L., Chandler C. J., 2010, *ApJ*, 712, 1403
- Pöppel W. G. L., Scalise E. Jr, 1989, *Rev. Mex. Astron. Astrofis.*, 17, 121
- Rao R., Girart J. M., Marrone D. P., Lai S., Schnee S., 2009, *ApJ*, 707, 921
- Ristorcelli I. et al., 2005, *Proc. IAU Symp. 231P Proc. IAU Symp. 231P, Astrochemistry: Recent Successes and Current Challenges, Poster sessions*, p. 227
- Slysh V. I., Val'tts I. E., Kalenskii S. V. et al., 1999, *A&ASS*, 134, 115
- Terebey S., Vogel S. N., Myers P. C., 1992, *ApJ*, 390, 181
- Torrelles J. M., Gómez J. F., Rodríguez L. F. Ho P. T. P., Curiel S., Vázquez S., 1997, *ApJ*, 489, 744
- Van der Wiel M. H. D., Jacobsen S. K., Jørgensen J. K., Bourke T. L., Kristensen L. E., 2019, *A&A*, 626A, 93
- Wilking B. A., Claussen M. J., 1987, *ApJ*, 320, L13
- Wilking B. A., Lada C. J., 1983, *ApJ*, 274, 698
- Wootten H. A., 1989, *ApJ*, 337, 858
- Yeh S. C. C., Hirano N., Bourke T. L. Ho P. T. P., Lee C.-F., 2008, *ApJ*, 675, 454

This paper has been typeset from a $\text{\TeX}/\text{\LaTeX}$ file prepared by the author.